EXTREMELY LOW CYCLE FATIGUE BEHAVIOUR OF HIGH STRENGTH 2024-T351 ALUMINUM ALLOY

Jakub JUDAS, Josef ZAPLETAL, Vít JAN

Brno University of Technology, Faculty of Mechanical Engineering, Brno, Czech Republic, EU,
Jakub.Judas@vutbr.cz

https://doi.org/10.37904/metal.2022.4497

Abstract

It has been found in recent years that the conventional Manson-Coffin law tends to overestimate the fatigue life at high levels of plastic loading. Such reduction in fatigue life is associated with a fundamental change in the mechanism of damage accumulation. Deterioration of the structure by cracks propagation becomes marginal and the fatigue resistance is governed by the ductility exhaustion phenomenon. The plastic deformation ability under extremely low cycle fatigue conditions is generally related to the occurrence of secondary phases, ie. inclusions and precipitates, dispersed in the matrix. This study investigates the microstructure of hardenable 2024 aluminum alloy and its effect on the cyclic response in the extremely low cycle fatigue region. Metallographic samples of the studied alloy were probed using SEM/EDS and EBSD analysis to identify the morphology and chemical composition of the observed phases. Fatigue tests were conducted in a symmetrical push-pull regime under strain control at room temperature and cyclic plasticity and S-N curves were determined. Electron microscopy observations revealed anisotropic microstructure with numerous fragmented inclusions. Fractographic analysis showed that these hard and brittle secondary phases act as an effective microstructural flaw leading to strong plastic damage accumulation and subsequently to fatigue cracks nucleation. In terms of fatigue life curves, a huge discrepancy in the fatigue data was observed at the extreme levels of cyclic straining. To overcome this shortcoming, a new three-parameter regression function was successfully employed and the obtained results were further discussed.

Keywords: Aluminum alloy 2024, inclusions, cyclic plasticity, low cycle fatigue, regression functions

1. INTRODUCTION

Aluminum alloys of the 2xxx series (Al-Cu-Mg) have proven to be technically advanced materials for a wide range of engineering applications, particularly in the aeronautical, automotive, and transportation sectors. The most common and most promising in this category is the 2024 hardenable aluminum alloy which is extensively applied due to its properties of high strength ratio, low density, and better thermal stability. Such materials may be subjected to a significant amount of plastic deformation during manufacturing and operation cycles, which can lead to their subsequent failure [1,2].

Ductile metal under periodic plastic loading often fails within a limited number of life cycles, approximately about 10^5. This phenomenon is called low-cycle fatigue (LCF) in a broad sense. In this regime, Manson and Coffin independently proposed the empirical fatigue law which is referred to as the Manson-Coffin relationship [3,4]. This equation is represented by a straight line on the log-log scale when the coordinates are the plastic strain range and the number of cycles to failure. In addition, under extreme seismic conditions, structural members acting as dissipative elements experience small numbers of very large displacement cycles. These loading conditions result in a rapid failure when the fracture occurs within about 100 cycles and the material performs differently from common LCF behaviour [5]. The fatigue process with such a short life is termed extremely low-cycle fatigue (ELCF).

An overestimation of fatigue life by the conventional Manson-Coffin law has been observed in the very low cycle region since the experimental curves are concave smoothly toward the vertical axis [6,7]. Such reduction in fatigue life corresponds to the transition of the damage accumulation mechanism. At the large level of strain field, the fatigue damage is dominated primarily by ductility exhaustion, and the crack initiation site is located in the interior of the specimen. On the other hand, in the LCF regime, the damage is represented by crack propagation and fatigue cracks starting from the surface [5,8].

Efforts have been made to overcome the shortcomings of the Manson-Coffin law in the ELCF regime [9,10,11]. These models are generally based on the concept of plastic damage due to ductility exhaustion during cyclic straining and provide good agreement with experimental data for many engineering alloys. More recently, Xue proposed an exponential function by combining the Manson-Coffin power law function with the plastic damage function, which universally fits the complete range of life cycles [12].

2. MATERIALS AND METHODS

In this study, a commercially available AA2024-T351 aluminum alloy in a 20 mm-thick plate was used. The element composition of the as-received material determined by a GDOES spectrometer is given in **Table 1**. To make microscopic observations, two perpendicular sections were cut from the as-received plate with an abrasive cutter and consequently prepared by standard metallographic techniques. The final polishing was conducted using 1 μm particle size diamond paste and consequently etched with Keller‘s Reagent to reveal the basic microstructure features.

Table 1 Chemical composition of the studied 2024-T351 aluminum alloy

Elements	Al	Si	Fe	Cu	Mn	Mg	Zn	Ti
(wt%)	Balance	0.07	0.25	4.3	0.52	1.71	0.01	0.04

Light microscope (LM, Zeiss Axio Observer, Germany) was employed for the initial characterization of metallographic samples. Fracture surfaces of broken specimens were analyzed via a scanning electron microscope in standard SE and BSE modes (ULTRA PLUS, Carl Zeiss, Germany). Energy-dispersive X-ray spectroscopy (Aztec, Oxford Instruments) was used for the chemical identification of secondary phases present in the alloy matrix. An EBSD analysis was further performed to determine the degree of grain anisotropy and the possible occurrence of deformation texture.

Static mechanical tests were carried out on a ZWICK Z250 testing device with a constant strain rate of 1 mm/min at room temperature. Strain-controlled cyclic testing was performed using triangle-shaped symmetrical loading with defined total strain amplitude (0.6 to 3 %) with a strain rate of 0.002 s^{-1}. The low-cycle fatigue tests were undertaken using INSTRON 8801 testing system with a 100 kN dynamic load cell and equipped with a clip-on dynamic strain extensometer (gauge length of 14 mm).

3. RESULTS AND DISCUSSION

3.1. Microstructure evaluation

The typical microstructure of the experimental material in the longitudinal orientation consists of solid solution grains containing alloying elements and a large number of inclusions arranged in the rolling direction (**Figure 1**). The EBSD investigation showed that the alloy matrix is composed of elongated grains with an average length and width of about 140 and 30 μm, respectively. Significant structure anisotropy is present even though the alloy has undergone a solution annealing treatment after the forming process. This unusual

behaviour can be explained by the pinning effect of grain boundary precipitates which inhibit boundary migration during recovery and recrystallization [13].

The 2024 aluminum alloy has a high content of alloying elements and therefore various secondary phases nucleate in the matrix. The EDS mapping of chemical composition revealed three types of phases that manifest in the microstructure (**Table 2**). The first category is a minor granular AlCuMg precipitate with a smooth edge. These are probably residues that did not have enough time to dissolve at the solution annealing temperature [14]. The second phase is a coarse AlCuFeMn copper-rich particle with a rough fringe and the highest tendency to fragment in the microstructure. Closer inspection of this impurity displayed distinct chemical segregation throughout its volume (region I and II). The last type is iron-rich AlFeMnCuSi inclusion with sharp-edged geometry. This intermetallic has the most detrimental effect on the mechanical properties due to the superposition of its high brittleness and stress concentration inducing geometry [15].

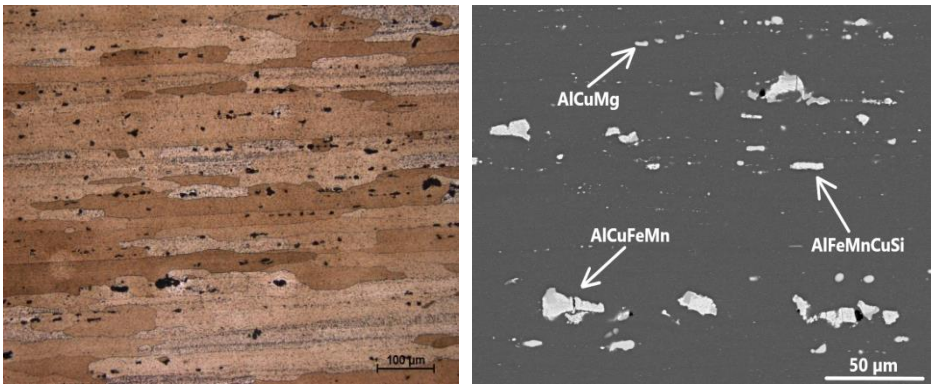

Figure 1 Microstructure of 2024-T351 alloy a) overall view (LM), b) detail of inclusions (SEM, BSE)

Table 2 EDS chemical composition of observed secondary phases

Elements (at%)	Al	Cu	Fe	Mn	Si	Mg
AlCuFeMn (global)	75	14	7	4	-	-
AlCuFeMn (region I)	73	18	6	3	-	-
AlCuFeMn (region II)	74	8	11	7	-	-
AlFeMnCuSi	76	5	8	6	5	-
AlCuMg	53	24	-	-	-	23

3.2. Static straining

The obtained mechanical results for static tensile and compression loading of the aluminum alloy are depicted in **Figure 2.** The determined values of basic mechanical properties are given in **Table 3**. According to the analysis of the static stress-strain response, the experimental material exhibits continuous elastoplastic transition with a similar value of proof stress for both loading conditions. The compression response shows noticeable higher ultimate strength and plasticity. The ratio of ultimate and yield strength (equals 1.6 for tension) indicates a strong static hardening ability, even though the material is in a high strength state due to forming process and subsequent heat treatment.

Table 3 Mechanical tensile and compression properties of 2024-T351 aluminum alloy

Material	E (GPa)	σ_y (MPa)	σ_{UTS} (MPa)	ε_t (%)	σ_{yC} (MPa)	σ_{UCS} (MPa)	ε_c (%)
2024-T351	72.5	301	471	18.8	322	1058	35.6

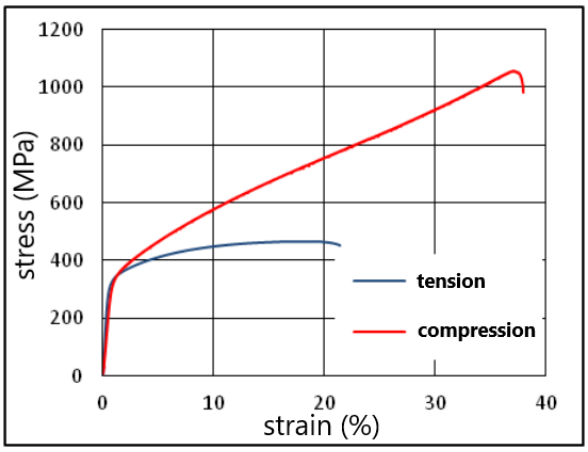

Figure 2 Mechanical testing results for static tensile and compression loading

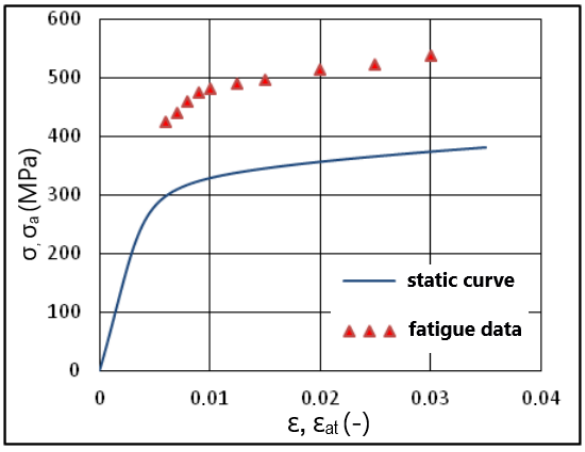

Figure 3 Static tensile curve and fatigue data for cyclic Ramberg-Osgood function

3.3. Cyclic plasticity and fatigue life curves

The hardening behaviour is confirmed by the comparison between monotonic and cyclic stress-strain curves which is based on an analysis of fatigue hysteresis loops for each strain amplitude. The cyclic stress-strain curve, which represents the plastic response of the material to alternating loading, was obtained by fitting the Ramberg-Osgood relationship to the experimental data [16]:

$$\varepsilon_{at} = \frac{\sigma_a}{E} + \left(\frac{\sigma_a}{K'}\right)^{1/n'} \quad (1)$$

where *E* is Young´s modulus, *K´* is the cyclic strength coefficient and *n´* is the cyclic strain hardening exponent. Shift of saturated stress values above the monotonic deformation curve clearly demonstrates the cyclic hardening ability of the alloy (**Figure 3**). This effect is connected with the evolution of strengthening dislocation substructure which is the result of large reserve of material plasticity prior to cyclic straining [17].

The experimental data in the LCF regime can be fitted using Manson-Coffin and Wöhler-Basquin law which can be linked together via linear deformation superposition, expressed in Morrow notation as:

$$\varepsilon_{at} = \frac{\sigma'_f}{E}\left(2N_f\right)^b + \varepsilon'_f\left(2N_f\right)^c \quad (2)$$

where ε'_f, σ'_f, *b* and *c* are known LCF parameters [4,16]. Plastic strain amplitude dependence on the number of cycles to failure is not described by the Manson-Coffin law sufficiently for the aluminum alloy at the large level of plastic strain field (**Figure 4**). Based on this phenomenon, an alternative Xue damage function is chosen to correct the general drawback of over-predicting the fatigue life under extremely low cycle fatigue conditions. The new exponential regression function can be rewritten in the form of:

$$\varepsilon_{ap} = \varepsilon_f \cdot \left[\frac{1}{\lambda} \cdot ln\left(\frac{e^{\lambda} - 1}{4N_f} + 1\right)\right]^{1/m} \quad (3)$$

where λ and *m* are progressive fatigue characteristics used for plotting strain-life curve covering the whole range of cyclic life [12]. The parameter ε_f can be successfully correlated with the value of fracture strain obtained from the monotonic tensile diagram. Derived conventional and advanced regression fatigue constants with transition life N_t are listed in **Table 4**.

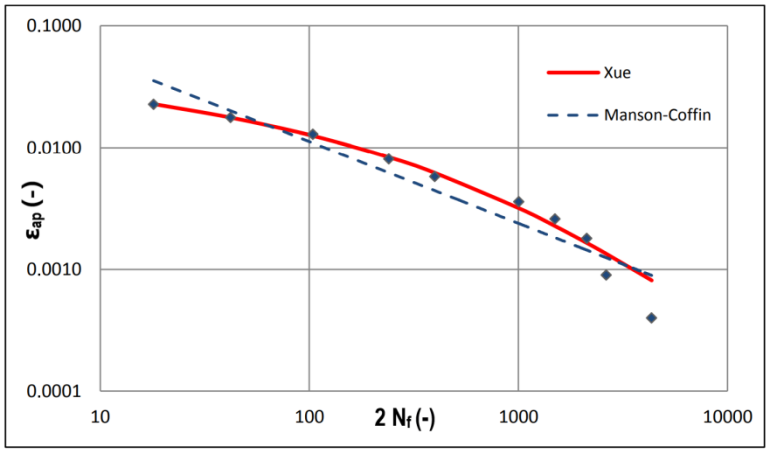

Figure 4 Modified strain-life curve of 2024-T351 alloy

Table 4 Derived fatigue regression parameters of the experimental material

σ_f' (MPa)	b (-)	ε_f' (-)	c (-)	ε_f (-)	λ (-)	m (-)	N_t (-)
609.42	-0.038	0.247	-0.671	0.0655	9.108	0.537	104

3.4. Fractographic analysis

Fracture surfaces of the specimens broken during cyclic loading are shown in **Figure 5**. Fatigue crack initiation close to the specimen surface in the vicinity of larger inclusion was characteristic for all the applied strain amplitudes. A more detailed EDS measurement revealed iron-rich secondary phases with sharp-edged geometry. The presence of these hard and brittle inclusions is an effective microstructural flaw leading to strong plastic damage accumulation inside the material [8,17]. Local plasticity exhaustion at the site of inclusions subsequently facilitates crack nucleation and its growth [18]. Transcrystalline fatigue striations were a characteristic feature observed near the crack initiation region. Increasing the plastic strain amplitude reduced the frequency of fatigue striations, which is in good agreement with the accelerated stage of fatigue crack growth in the ELCF regime [7,8].

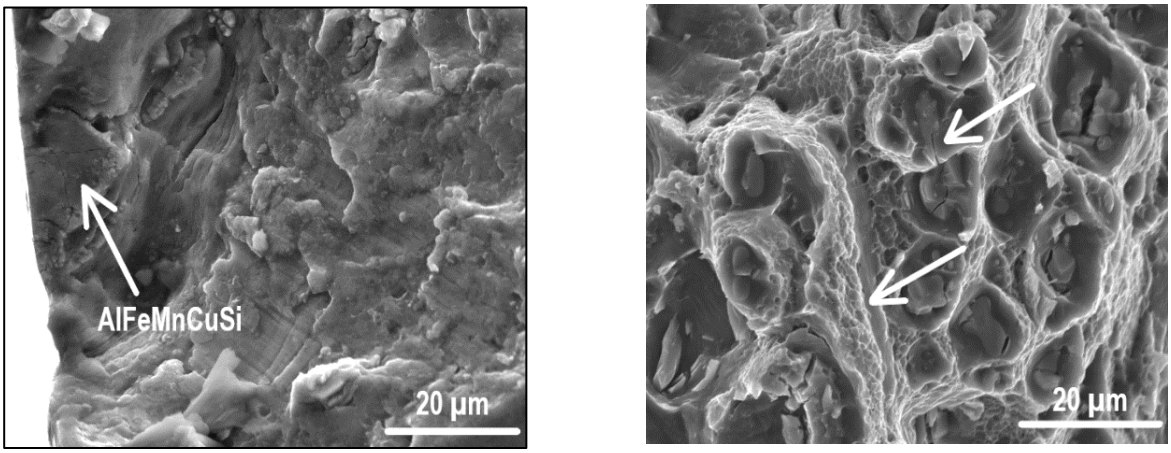

Figure 5 SEM fractographs of 2024-T351 aluminum alloy (ε_{at} = 1.5 %), a) crack initiation site with marked surface inclusion, b) ductile fracture region with dimple morfology

The final fracture area has a typical appearance of a ductile failure mechanism at all loading amplitudes. Due to the occurrence of larger inclusions and fine precipitates, two size levels of dimples were observed on the

fracture surface. Secondary phases were present in the ductile dimples, while some of the particles were broken due to the applied plastic deformation. Decohesion of inclusions from the surrounding solid solution is also evident in some places, indicating insufficient wettability of the alloy matrix. The overall observation of the fatigue fracture surface thus clearly proves the key role of micro-purity on the fatigue performance of the 2024-T351 aluminum alloy.

4. CONCLUSIONS

- Microstructure of the rolled 2024-T351 aluminum alloy consists of solid solution grains and a large number of secondary phases arranged in the forming direction.
- EDS mapping revealed three types of phases dispersed in the matrix, residues of AlCuMg precipitates, coarse AlCuFeMn particles exhibiting chemical segregation, and brittle AlFeMnCuSi inclusions with sharp-edged geometry.
- The monotonic stress-strain response exhibits continuous elastoplastic transition with a similar value of proof stress for both loading conditions.
- The comparison between monotonic and cyclic stress-strain data clearly demonstrates the cyclic hardening ability of the alloy for all of the applied strain amplitudes.
- Conventional Manson-Coffin law does not sufficiently describe the strain-life curve in the extremely low cycle regime, therefore a more convenient exponential function based on Xue plastic damage model is applied.
- Fatigue crack initiation site in the vicinity of iron-rich inclusion was found in all tested specimens. The incidence of observed transcrystalline fatigue striations diminishes with increasing amplitude of cyclic deformation.
- The final fracture shows typical features of ductile failure with two size levels of dimples due to the occurrence of fragmented inclusions and fine precipitates. Decohesion of secondary phases from the matrix is another potential mechanism of fatigue damage.

REFERENCES

[1] ASHKENAZI, D. How aluminum changed the world: A metallurgical revolution through technological and cultural perspectives*. Technological Forecasting and Social Change*. 2019, vol. 143, pp. 101-113.

[2] HUDA, Z., TAIB, N.I., ZAHARINIE, T. Characterization of 2024-T3: An aerospace aluminum alloy. *Materials Chemistry and Physics.* 2009, vol. 113, pp. 515-517.

[3] MANSON, S.S. Behaviour of materials under conditions of thermal stress. *National Advisory Committee for Aeronautics*. 1954, vol. 1170, pp. 317-350.

[4] COFFIN, L.F. A study of the effects of cyclic thermal stresses on a ductile metal. *Transactions of the ASME*. 1954, vol. 76, pp. 931-50.

[5] SHIMADA, K., KOMOTORI, J., SHIMIZU, M. Fracture mode transition and damage in extremely low cycle fatigue. In: *Second International Conference on Low Cycle Fatigue and Elasto-Plastic Behavior of Materials*. 1987, pp. 68-71.

[6] COFFIN, L.F. A note on low cycle fatigue laws. *J Mater JMLSA*. 1971, vol. 6, pp. 388-402.

[7] WANG, L. et al. Low-cycle fatigue testing of extruded aluminum alloy buckling restrained braces. *Engineering Structures*. 2013, vol. 46, pp. 294-301.

[8] KANVINDE, A.M., DEIERLEIN, G.G. Continuum based micro models for ultra-low cycle fatigue crack initiation in steel structures. In: *Proceedings of the 2005 structures congress*. New York, 2005, pp. 4-20.

[9] Kuroda, M. Extremely low cycle fatigue life prediction based on new cumulative fatigue damage model. *Internation Journal of Fatigue*. 2002, vol. 24, pp. 699-703.

[10] TATEISHI, K., HANJI, T., MINAMI, K. A prediction model for extremely low cycle fatigue strength of structural steel. *Internation Journal of Fatigue*. 2007, vol. 29, pp. 887-896.

[11] CHEN, L. et al. Power exponent function model for low cycle fatigue life prediction and its applications. *International Journal of Fatigue*. 2007, vol. 29, pp. 1-9.

[12] XUE, L. A unified expression for low cycle fatigue and extremely low cycle fatigue and its implication for monotonic loading. *International Journal of Fatigue*. 2008, vol. 30, pp. 1691-1698.

[13] GOLOBORODKO, A. et al. Friction Stir Welding of a Commercial 7075-T6 Aluminum Alloy. *Materials Transactions*. 2004, vol. 45, pp. 2503-2508.

[14] SHEN, Z. et al. The structure determination of $Al_{20}Cu_2Mn_3$ by near atomic resolution chemical mapping. *Journal of Alloys and Compounds.* 2014, vol. 601, pp. 25-30.

[15] JIN, Y. et al. The anisotropy of fatigue crack nucleation in an AA7075 T651 Al alloy plate. *Materials Science and Engineering*. 2015, vol. 622, pp. 7-15.

[16] BASAN, R. et al. Study on Ramberg-Osgood and Chaboche models for 42CrMo4 steel and some approximations. *Journal of Constructional Steel Research*. 2017, vol. 136, pp. 65-74.

[17] SURESH, S. *Fatigue of Materials*. Cambridge University Press, 1991.

[18] WISNER, B., KONTSOS, A. Investigation of particle fracture during fatigue of aluminum 2024. *International Journal of Fatigue*. 2018, vol. 111, pp. 33-43.